

Short-time Fatigue-Life Estimation for Non-Stationary Processes Considering Structural Dynamics

Aleš Zorman^a, Janko Slavič^{a,*}, Miha Boltežar^a

^aUniversity of Ljubljana, Faculty of Mechanical Engineering, Aškerčeva 6, 1000 Ljubljana, Slovenia

Cite as:

Aleš Zorman, Janko Slavič, and Miha Boltežar, Short-time Fatigue-Life Estimation for Non-Stationary Processes Considering Structural Dynamics, International Journal of Fatigue, 106178, <https://doi.org/10.1016/j.ijfatigue.2021.106178>

Abstract

Structural dynamics relates the excitation profile to the dynamic loads at a particular location of the structure. Spectral methods fatigue-life estimation is based on the assumptions of stationarity and the Gaussianity. This research proposes a method for a fatigue-life estimation for non-stationary excitation. The method is based on the short-time spectral narrowband method, where the short-time width was found to be related to the structural dynamics (i.e., natural frequency, damping) of the excited structure. A detailed numerical and a real experiment shows a significant accuracy increase for fatigue-life estimation at non-stationary and non-Gaussian excitation.

Keywords: fatigue life; random loads; non-stationarity; narrowband; short-time

1. Introduction

In vibration fatigue flexible structures are subjected to irregular loads that are amplified at the system's natural frequencies and therefore have a significant effect on the fatigue life [38].

In general, two approaches to a fatigue-damage estimation exist. The first

*Corresponding author

Email address: janko.slavic@fs.uni-lj.si (Janko Slavič)

is a time-domain analysis, where stress cycles are extracted from a known time history by employing cycle-counting methods. One of the most widely used counting methods is the rainflow algorithm, introduced by Matsuishi and Endo [22, 2]. According to the hypothesis of linear damage accumulation, known as the Palmgren-Miner rule [30], the fatigue-life is estimated. The second approach is in the frequency domain [38]. If a Gaussian distribution and the stationarity of the analyzed time histories are assumed, the power spectral density (PSD) uniquely defines the statistical characteristics of the time history [28]. In recent years, a lot of effort was put into the investigation of spectral methods, since they provide several advantages (*e.g.*, statistical description of loads, significantly faster numerical simulations). Initially, in the frequency domain, counting methods have been researched, see *e.g.*: [14, 25, 15], but in the recent years multiaxial [3, 10, 29, 24], non-Gaussian [31, 41, 13] and non-stationary [43, 40, 19] loads have attracted much attention. This research is focused on non-Gaussian and non-stationary loads, *e.g.*, originating from pressure fluctuations in aeronautics applications [1] or road irregularities [35].

Kihm *et al.* [16] numerically demonstrated that a dynamic system's response to stationary, non-Gaussian excitation is Gaussian, justifying the use of frequency-counting methods. This phenomenon does not apply to nonlinear systems due to the violation of the central limit theorem [6]. Due to the heavy tailed cycle amplitude probability density function (PDF) of the non-Gaussian stress response, spectral methods underestimate the damage intensity [16]. Bracessi *et al.* [7] proposed a correction formula for the steady non-Gaussian stress state, which was later improved by Cianetti *et al.* [13] for the strongly non-Gaussian stress state. Benasciutti *et al.* [4] enhanced the Tovo-Benasciutti method to incorporate the effects of a non-Gaussian distribution of the stress load in terms of both skewness and kurtosis [39]. Wolfsteiner *et al.* [44] researched the fatigue-damage potential of non-Gaussian random vibration for multi-degree-of-freedom (MDOF) systems.

For non-stationary and non-Gaussian excitation, the bandwidth of the dynamic system's frequency-response function is of great importance; for the Gaus-

sian response, the period of the system’s impulse-response function has to be significantly longer than the occurrence rate of the load peaks [16]. Palmieri *et al.* [31] experimentally researched different rates of the non-Gaussian and non-stationary excitation of a dynamics system; similar to Kihm *et al.* [16], who found that for a dynamic system, the non-Gaussianity in excitation results in Gaussian loads. However, the non-stationarity in the excitation propagated to the non-stationarity in loads and significantly impacted on the fatigue life [16]. Capponi *et al.* [9] proposed a run-test approach and defined the non-stationarity index. In experimental work, the appropriate time-window width was related to the system’s impulse-response function (IRF) for the identification of excitation non-stationarity [9]. Cianetti *et al.* [12] researched the influence of different time-window parameters on a fatigue damage-estimation for applications of monitoring the instantaneous fatigue.

Considerable research effort was put into extending the existing spectral methods for the non-stationary and non-Gaussian loads. Benasciutti *et al.* [5] researched switching loads, where they employed a frequency-based analysis of each adjacent stationary Gaussian or non-Gaussian segment. Wolfsteiner analyzed the decomposition of non-stationary random vibrations into Gaussian portions with direct applicability to frequency-counting methods [43]. Trapp *et al.* studied an extension of the frequency-domain approach to the fatigue assessment of amplitude-modulated non-stationary loading [40]. Furthermore, the non-stationarity matrix was introduced by Trapp *et al.* [42] to encompass the non-stationarity of loading’s frequency content.

Zhou *et al.* [45] numerically investigated stress mode shapes for the prediction of multi-axial random fatigue hotspots. It was shown that the majority of the response energy is concentrated in the vicinity of the mode shape, which is predominant at the fatigue hotspot. The latter was exploited in thermoelasticity-based modal damage identification by Capponi *et al.* [8], where the damage intensity of a particular mode shape was determined on the basis of a narrow-band response approximation.

This study researches the effect of the system’s dynamic properties (*i.e.*, nat-

ural frequency, damping ratio) on how the non-stationary excitation propagates through the dynamic system to the (non-stationary) load. The stress load at the fatigue hotspots is considered narrowband and the fatigue-life is estimated using a short-time principle. The applicability of the proposed method to various non-stationary excitations is numerically and experimentally researched.

This manuscript is organized as follows. In Section 2 a theoretical background for random processes, structural dynamics and damage evaluation is provided. Section 3 introduces a method for a multiaxial fatigue-life estimation of a structure subjected to a non-stationary and non-Gaussian random excitation. In Section 4 numerical research and application of the proposed method is provided, and additional experimental research is given in Section 5. Section 6 draws the conclusions.

2. Theoretical background

In this section the theoretical background to the random process, structural dynamics and frequency-domain fatigue estimation will be given.

2.1. Random process properties

In vibration fatigue, structures are subjected to deterministic and non-deterministic loads and can be researched as a random process [6, 38]. A random process $x(t)$ is characterized by the PDF as a function of a random variable x and time t :

$$p(x, t) = \lim_{\Delta x \rightarrow 0} \frac{P(x \leq x(t) \leq x + \Delta x)}{\Delta x}. \quad (1)$$

The definition refers to an ensemble $\{x(t)\}$, where each sample function corresponds to a random variable x at time t . For the purpose of mathematical manageableness, assumptions of ergodicity and stationarity are made, although they are not always justified [6]. A stochastic process is weakly ergodic if the time averages equal the ensemble averages with respect to the mean and the covariance function [37]. For the random process to be considered stationary, its probability distribution must be time independent [28].

A Gaussian-distributed random process is described by the PDF $p(x, t)$ [28]:

$$p(x, t) = \frac{1}{\sqrt{2\pi\sigma^2(t)}} e^{-\frac{(x-\mu(t))^2}{2\sigma^2(t)}}, \quad (2)$$

which has two degrees of freedom and is fully defined by the first statistical moment, representing time dependent mean value $\mu(t)$ (definition in a broad sense, corresponding to an ensemble average) or for ergodic random process, representing time independent mean value μ :

$$\mu(t) = E[x(t)] = \frac{1}{o} \sum_{p=1}^o x_p(t), \quad (3a)$$

$$\mu = \langle x(t) \rangle = \frac{1}{n} \sum_{i=1}^n x_i, \quad (3b)$$

and the variance $\sigma^2(t) = M_2(t)$ [28], which is defined by the second ($j = 2$) central statistical moment [37]:

$$M_j(t) = E[(x(t) - \mu(t))^j] = \frac{1}{o} \sum_{p=1}^o (x_p(t) - \mu(t))^j, \quad (4a)$$

$$M_j = \langle (x(t) - \mu)^j \rangle = \frac{1}{n} \sum_{i=1}^n (x_i - \mu)^j. \quad (4b)$$

In Eqs. (3) and (4) o and n are the number of ensemble functions and number of data points in the discrete time series, respectively.

Although it is common to assume Gaussianity, since, due to the central limit theorem [6], many physical processes exhibit a Gaussian probability distribution, some real loading cases do manifest non-Gaussianity. Parameters describing the non-Gaussianity are skewness s_k and kurtosis k_u :

$$s_k = \frac{M_3}{M_2^{3/2}} = \frac{M^3}{\sigma^3}, \quad k_u = \frac{M_4}{M_2^2} = \frac{M^4}{\sigma^4}. \quad (5)$$

Skewness, s_k , is a measure of the asymmetry of the probability distribution, whereas kurtosis, k_u , meters the sharpness of the PDF. For a Gaussian-distributed random process, kurtosis has a value of 3. A process is considered to be platykurtic for values $k_u < 3$ and to be leptokurtic for $k_u > 3$ [28].

2.2. Structural dynamics and modal reduction

When dealing with the response of flexible structures, the majority of fatigue damage is accumulated around the system's excited natural frequencies. To relate a system's stress response with its excitation, the stress frequency-response function (FRF) is used [17]. The following paragraphs provide the minimal theory with regard to structural dynamics. For more details the reader is referred to [38].

A linear, time-invariant, MDOF system is described with equations of motion:

$$\mathbf{M}\ddot{\mathbf{x}}(t) + \mathbf{C}\dot{\mathbf{x}}(t) + \mathbf{K}\mathbf{x}(t) = \mathbf{f}(t) \quad (6)$$

where \mathbf{M} , \mathbf{C} and \mathbf{K} are the mass, viscous damping and stiffness matrices, respectively. $\mathbf{x}(t)$ and $\mathbf{f}(t)$ are the time-dependent displacement and excitation force vectors, respectively. Generally, Eq. (6) represents a coupled system of differential equations. For lightly damped systems, the use of proportional damping is appropriate and the equations of motion can be decoupled with a transition to modal coordinates $\mathbf{q}(t)$ [20]:

$$\mathbf{I}\ddot{\mathbf{q}}(t) + \begin{bmatrix} \diagdown & & \\ & 2\xi_r\omega_r & \\ & & \diagdown \end{bmatrix} \dot{\mathbf{q}}(t) + \begin{bmatrix} \diagdown & & \\ & \omega_r^2 & \\ & & \diagdown \end{bmatrix} \mathbf{q}(t) = \mathbf{\Phi}^T \mathbf{f}(t) \quad (7)$$

with the relation between the physical and modal coordinates given as [20]:

$$\mathbf{x}(t) = \mathbf{\Phi}\mathbf{q}(t). \quad (8)$$

In Eq. (7), \mathbf{I} represents the identity matrix, $2\xi_r\omega_r$ denotes the mass-normalized r -th damping element and ω_r^2 is the square of the r -th natural frequency. The mass-normalized modal matrix $\mathbf{\Phi}$ consists of N vertically stacked mass-normalized eigenvectors $\mathbf{\Phi}_r$ that are complementary to the eigenvalues ω_r^2 in a solution to the N -DOF system eigenvalue problem:

$$(\mathbf{K} - \omega^2\mathbf{M})\mathbf{X} = \mathbf{0}. \quad (9)$$

By employing the system modal model, *i.e.*, modal matrix $\mathbf{\Phi}$, the system eigenfrequencies ω_r and the damping ratios ξ_r , receptance matrix $\mathbf{H}(\omega)$ can be ex-

pressed in diagonal form [38, 20]:

$$\mathbf{H}(\omega) = \mathbf{\Phi} \left[\begin{array}{c} \diagdown \\ \omega_r^2 - \omega^2 + i 2 \xi_r \omega \omega_r \\ \diagup \end{array} \right]^{-1} \mathbf{\Phi}^T. \quad (10)$$

For a vibration fatigue damage assessment the stress response $\mathbf{X}_s(\omega)$ is required. By employing a finite-element method (FEM) analysis, the i -th component of the stress steady-state response $\mathbf{X}_{s_i}(\omega)$ is readily obtained from the displacement response under the assumption of small deflections using Hooke's law [38]:

$$\mathbf{X}_{s_i}(\omega) = \mathbf{\Phi}_{s_i} \left[\begin{array}{c} \diagdown \\ \omega_r^2 - \omega^2 + i 2 \xi_r \omega \omega_r \\ \diagup \end{array} \right]^{-1} \mathbf{\Phi}^T \mathbf{F}(\omega) = \mathbf{H}_{s_i f}(\omega) \mathbf{F}(\omega) \quad (11)$$

with $\mathbf{\Phi}_{s_i}$ and $\mathbf{H}_{s_i f}(\omega)$ representing the i -th stress-component modal matrix and the stress-component FRF, respectively. The stress components s_i constitute the stress tensor \mathbf{s} using Voigt vector notation:

$$\mathbf{s} = [s_{xx}, s_{yy}, s_{zz}, s_{xy}, s_{yz}, s_{xz}]. \quad (12)$$

The stress modal matrix $\mathbf{\Phi}_s$ is defined via the stiffness tensor \mathbf{C} and the linear spatial differential operator $D\{\cdot\}$ [38]:

$$\mathbf{\Phi}_s = \mathbf{C} D\{\mathbf{\Phi}\}, \quad (13)$$

where $D\{\cdot\}$ is defined as:

$$D\{\cdot\} = \frac{1}{2} (\nabla + \nabla^T). \quad (14)$$

The stress component FRF $\mathbf{H}_{s_i f}(\omega)$ containing N modes is expressed as:

$$\mathbf{H}_{s_i f}(\omega) = \sum_{r=1}^N {}_r \mathbf{H}_{s_i f}(\omega) = \sum_{r=1}^N \frac{{}_r \mathbf{R}^{s_i}}{\omega_r^2 - \omega^2 + i 2 \xi_r \omega \omega_r}, \quad (15)$$

where ${}_r \mathbf{H}_{s_i f}$ and ${}_r \mathbf{R}^{s_i}$ are the r -th modal and i -th stress component FRF and the modal constant matrix [17], respectively.

For a description of the random excitation and the i -th stress-component response in the frequency domain, the power spectral density (PSD) is used:

$$\mathbf{S}_{s_i s_i}(\omega) = |\mathbf{H}_{s_i f}^*(\omega)|^2 \cdot \mathbf{S}_{ff}(\omega) \quad (16)$$

with $\mathbf{S}_{s_i s_i}(\omega)$ and $\mathbf{S}_{ff}(\omega)$ being the i -th stress component PSD and the force excitation PSD, respectively. A generalized form can be used to include the cross-correlation terms, known as the stress spectral density matrix or the stress cross-correlation matrix [38]:

$$\mathbf{S}_{ss}(\omega) = \mathbf{H}_{sf}^*(\omega) \cdot \mathbf{S}_{ff}(\omega) \cdot \mathbf{H}_{sf}^T(\omega), \quad (17)$$

where the stress frequency-response function vector is defined as [38, 6]:

$$\mathbf{H}_{sf}(\omega) = [\mathbf{H}_{s_1 f}(\omega), \mathbf{H}_{s_2 f}(\omega), \mathbf{H}_{s_3 f}(\omega), \mathbf{H}_{s_4 f}(\omega), \mathbf{H}_{s_5 f}(\omega), \mathbf{H}_{s_6 f}(\omega)]. \quad (18)$$

When a structure is excited in a limited frequency range, only a subset u of N modes can be considered. A common frequency range, *e.g.*, for automotive accelerated-vibration test procedure is 5-2 000 Hz, making the higher frequency modes negligible, and so they can thus be omitted using the modal decomposition [27]:

$$\tilde{\mathbf{H}}_{s_i f}(\omega) = \sum_{r=1}^{u < N} r \mathbf{H}_{s_i f}(\omega). \quad (19)$$

Using the Eq. (19), the stress spectral density matrix (17) can be approximated as [27]:

$$\tilde{\mathbf{S}}_{ss}(\omega) = \tilde{\mathbf{H}}_{sf}^*(\omega) \cdot \mathbf{S}_{ff}(\omega) \cdot \tilde{\mathbf{H}}_{sf}^T(\omega) \approx \sum_{r=1}^{u < N} r \mathbf{H}_{sf}^*(\omega) \cdot \mathbf{S}_{ff}(\omega) \cdot r \mathbf{H}_{sf}^T(\omega). \quad (20)$$

2.3. Vibration fatigue damage estimation

For a time-domain fatigue-damage estimation the Palmgren-Miner [30, 23] linear cumulative damage rule is preferred, where each cycle at stress amplitude s_a is associated with a damage D_i :

$$D = \sum_{i=1}^l D_i = \sum_{i=1}^l \frac{n_i(s_a)}{N_i(s_a)}. \quad (21)$$

In Eq. (21) D is the total damage, l is the total number of blocks of constant-stress amplitude s_a , and n_i and N_i are the number of cycles and the number of cycles to failure at amplitude s_a , respectively. In theory, the total damage at

failure is often defined as $D = 1$. The Palmgren-Miner hypothesis is a stress-fatigue model that utilizes the S-N curve for a description of the material's resistance to fatigue [18]:

$$s_a^k N = C, \quad (22)$$

where k is the curve slope and C is the curve intercept. When taking the time-domain approach to fatigue analysis, the stress time history is reduced to a set of stress reversals with the corresponding mean stresses, usually with the rainflow-counting method [22]. The stress range PDF is obtained from the resulting range-mean cycle-counting matrix, and the damage intensity can be assessed [18].

Alternatively, the statistical properties of the stress time history can be described in the frequency domain by the moments of the stress response PSD, making the latter appropriate for a damage-intensity assessment [28].

For the majority of vibrating structures the failure is subjected to multi-axial random stress loading, described by the PSD of the reduced response $\tilde{\mathbf{S}}_{ss}(\omega)$. Using the modal-reduction approximation [27], the equivalent von Mises stress (EVMS) criterion, proposed by Pitoiset and Preumont [32], can be adopted:

$$\tilde{\mathbf{S}}_c(\omega) = \sum_{r=1}^{u < N} r \mathbf{S}_c(\omega), \quad (23)$$

where $r \mathbf{S}_c(\omega)$ relates to the r -th mode of the $\tilde{\mathbf{S}}_c(\omega)$ and is defined as [32]:

$$r \mathbf{S}_c(\omega) = \text{Trace}[\mathbf{Q} \cdot r \mathbf{S}_{ss}(\omega)], \quad (24)$$

In Eq. (24), \mathbf{Q} is a matrix of constant coefficients and is, in the case of planar stress, given as:

$$\mathbf{Q} = \begin{bmatrix} 1 & -1/2 & 0 \\ -1/2 & 1 & 0 \\ 0 & 0 & 3 \end{bmatrix}. \quad (25)$$

For a review of multiaxial fatigue criteria the reader is referred to [10]. The generalized form of the i -th spectral moment for the reduced mode r of the

EVMS stress is defined [38, 26]:

$${}_r\mathbf{m}_i = 2 \int_0^\infty \omega^i {}_r\mathbf{S}_c(\omega) d\omega. \quad (26)$$

3. Fatigue life for non-stationary processes

The fatigue failure of a vibrating system is generally a consequence of a material's deterioration in a localized areas, *i.e.*, in the hotspots. As discussed in Sec. 2.2, hotspots can be researched with the modal-decomposition concept and therefore decomposed for each deflection mode, see also [8, 26]. Here, the following hypothesis is made: it is reasonable to assume that the hotspots of the different EVMS stress mode shapes are spatially isolated and do not superimpose on each other. In application, this assumption should be checked through the stress modal analysis. In such a decomposed system, the majority of the system response damage is at the hotspot's predominant mode shape [45]. Consequently, the stress response at the hotspots can be approximated as a narrowband process [6, 8]. While the following theory will be deduced in vector form and for all the nodes of the structure, it is important to note that it is a valid approximation of the fatigue damage at the hotspots only.

The EVMS stress response ${}_r s_c(t)$ at the r -th mode shape's hotspot, represented by ${}_r\mathbf{S}_c(\omega)$ (24), is considered as a narrowband process with the stress cycle amplitude s_a being Rayleigh distributed [28]:

$$p(s_a) = \frac{s_a}{\sigma^2} e^{-\frac{s_a^2}{2\sigma^2}} \quad (27)$$

with σ^2 denoting mean square of stress response ${}_r s_c(t)$. However, when the excitation is non-stationary, Eq. (27) is rewritten using the short-time Δt stationary stress-response variance $\sigma^2(\Delta t)$, see Fig. 1a):

$$p(s_a, \Delta t) = \frac{s_a}{\sigma^2(\Delta t)} e^{-\frac{s_a^2}{2\sigma^2(\Delta t)}}. \quad (28)$$

The variance $\sigma^2(\Delta t)$ can be expressed in terms of the zeroth spectral moment (26) [38]:

$$\sigma^2(\Delta t) = {}_r\mathbf{m}_0(\Delta t) = 2 \int_0^\infty {}_r\mathbf{S}_c(\omega, \Delta t) d\omega, \quad (29)$$

where the vector $\boldsymbol{\sigma}^2(\Delta t)$ describes the variance at all nodes of the structure. The r -th EVMS stress response PSD ${}_r\mathbf{S}_c(\omega, \Delta t)$ can be estimated using the short-time Fourier transform (STFT). In time-frequency analysis, a compromise between time and frequency resolution has to be made, due to uncertainty principle theorem [21].

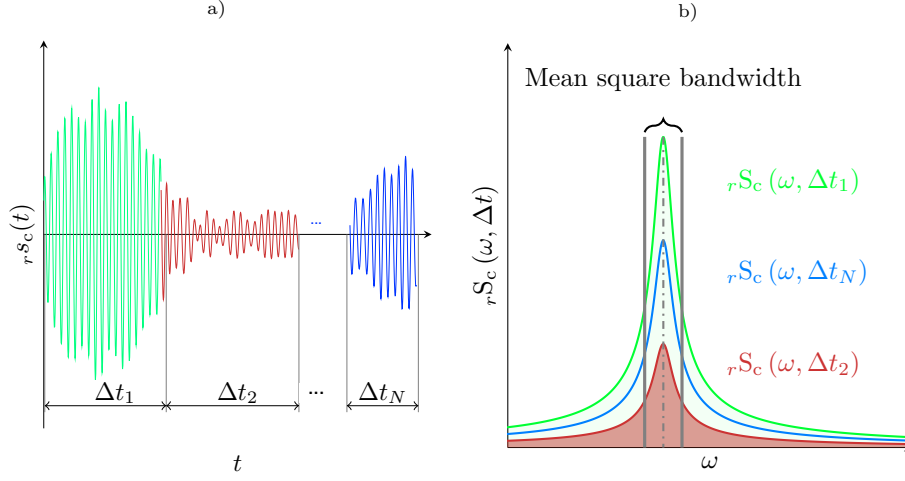


Figure 1: Narrowband stress response to non-stationary excitation: a) time history ${}_r\mathbf{s}_c(t)$; b) narrowband approximation of PSD ${}_r\mathbf{S}_c(\omega, \Delta t)$

As ${}_r\mathbf{S}_c(\omega)$ (24) describes the time-domain stationary random process of the uniaxial equivalent alternating von Mises stress ${}_r\mathbf{s}_c(t)$ [33], the variance (29) could also be obtained directly in the time domain (as will be the case in the later introduced short-time method). If the stress response ${}_r\mathbf{s}_c(t)$ is further decomposed into the r -th mode EVMS stress modal shape ${}_r\mathbf{s}_c$ and the time-dependent modal coordinate $q_r(t)$ (see also Eq. (8)):

$${}_r\mathbf{s}_c(t) = {}_r\mathbf{s}_c q_r(t), \quad (30)$$

the variance of ${}_r\mathbf{s}_c(t)$ can be expressed as:

$$\boldsymbol{\sigma}^2(\Delta t) = {}_r\mathbf{s}_c \boldsymbol{\sigma}_{q_r}^2(\Delta t), \quad (31)$$

where $\sigma_{q_r}^2(\Delta t)$ denotes variance of r -th modal coordinate at time segment Δt , given by Eq. (4b) for $j = 2$. Consequently, the estimation of the response variance is performed on the modal coordinate $q_r(t)$, which in general does not have to be a stationary random process.

Focusing on the r -th vibration mode, the r -th modal response $q_r(t)$ is obtained by convolution (denoted by $*$) of the corresponding mode's impulse-response function (IRF) $h_r(t)$ and the r -th modal excitation $f_r(t)$ [38, 20]:

$$q_r(t) = h_r(t) * f_r(t) = \int_{-\infty}^t h_r(t - \tau) f_r(\tau) d\tau. \quad (32)$$

In Eq. (32), $f_r(t)$ is given as $\Phi_r^T \mathbf{f}(t)$ (7) and $h_r(t)$ is characterized by the r -th modal mass m_r , the natural frequency ω_r and the damping ratio ξ_r :

$$h_r(t) = \frac{1}{m_r \omega_{d,r}} e^{-\xi_r \omega_r t} \sin \omega_{d,r} t, \quad (33)$$

where the damped natural frequency is given as $\omega_{d,r} = \omega_r \sqrt{1 - \xi_r^2}$ [20].

If the short-time stationarity assumption is used (29), then it is of critical importance to find the proper time Δt (if it exists). For the majority of physical phenomena, non-stationarity is exhibited as time fluctuations of their power as opposed to the less commonly observed non-stationary frequency content of the loading [9]. As shown in Fig. 2, the frequency of the excitation signal's power fluctuations (bursts) has a major effect on the stress load: the green color shows the case when the period of bursts in the excitation is long (relative to $h_r(t)$); in this case the bursts are completely transferred to the system response load and the process is non-stationary. However, when there are several bursts within envelope of $h_r(t)$, the response loads are averaged to a stationary process (blue color in Fig. 2). Fig. 2 depicts particular case of non-stationary excitation, where local burst are superimposed on stationary signal. For generalization, non-stationary excitation with various frequency content of modulating signal will be considered in search of short-time width Δt in Sec. 4.

As shown in Fig. 2 the proper short-time Δt depends on the properties of the dynamic system $h_r(t)$, *i.e.*, the natural frequency and the damping.

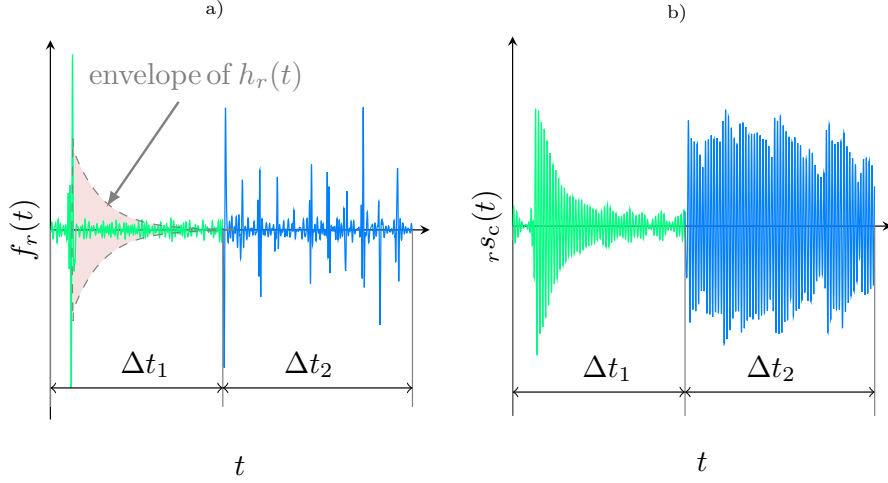


Figure 2: Effect of IRF $h_r(t)$ on the stress response non-stationarity: a) excitation; b) response load

Kihm *et al.* [16] researched how the non-Gaussian excitation propagates through the dynamic system. To discuss the details of the Kihm *et al.* research, the time T_w required for the envelope of $h_r(t)$ to drop to the fraction δ of the initial value has to be defined:

$$T_w = \frac{\ln(1/\delta)}{\omega_r \xi_r}, \quad (34)$$

where ω_r is the undamped natural frequency and ξ_r is the damping ratio. Kihm *et al.* [16] numerically found that the distribution of the system response tends towards Gaussian if the period of bursts in the excitation is shorter than 1/4 of time for the IRF to drop to 10 percent of its initial amplitude (*i.e.*, $\Delta t < T_w/4$, see Eq. (34) for $\delta = 0.1$). However, if the period of bursts is longer than $10 T_w$ for $\delta = 0.1$, the input kurtosis is reproduced in the response load.

In this research the time window Δt , required for the short-time variance $\sigma^2(\Delta t)$ estimation, will be researched in detail in a numerical simulation and is defined as:

$$\Delta t = n T_w, \quad (35)$$

where n denotes a fraction of T_w .

Using a short-time cycle amplitude PDF (28), the short-time damage intensity d [39, 36] is defined here as:

$$d_{\text{NB}}(\Delta t) = \nu_p C^{-1} \int_0^\infty s_a^k p(s_a, \Delta t) ds, \quad (36)$$

where C and k are material S-N curve parameters. A closed-loop expression for Eq. (36) is provided in Appendix Appendix A. In Eq. (36) the expected peak occurrence frequency ν_p coincides with the hot-spot predominant r -th stress mode shape's natural frequency [8]:

$$\nu_p = \frac{\omega_r}{2\pi}. \quad (37)$$

The average short-time-based damage-intensity estimator $\bar{d}_{\text{NB},\Delta t}$ of the non-stationary stress time history is obtained by time-averaging (denoted by $\langle \cdot \rangle$), according to Eqs. (3b) and (4b)) the expression, given by Eq. (36):

$$\bar{d}_{\text{NB},\Delta t} = \langle d_{\text{NB}}(\Delta t) \rangle = \nu_p C^{-1} \int_0^\infty s_a^k \langle p(s_a, \Delta t) \rangle ds, \quad (38)$$

as the short-time variance $\sigma^2(\Delta t)$ is considered to be a random process. The fatigue-life estimator is expressed as the inverse of the average damage intensity:

$$\bar{T}_{\text{NB},\Delta t} = \frac{1}{\bar{d}_{\text{NB},\Delta t}}. \quad (39)$$

The influence of short-time Δt on the fatigue-life error is examined with respect to the minimization of the fatigue-life error, defined as:

$$T_{\text{err}} = \frac{\bar{T}_{\text{NB},\Delta t} - T_{\text{RFC}}}{T_{\text{RFC}}}, \quad (40)$$

where T_{RFC} is the reference time-domain rainflow-counting algorithm used with the Palmgren-Miner rule.

4. Numerical research

In the following subsections the generation of excitation with various non-stationarity rates is presented and then the effect of the system's modal properties on the stress response is investigated with the aim to determine the proper short-time Δt width (35) for the fatigue-life estimation, using the proposed method of Sec. 3.

4.1. Non-stationary signal generation

Non-stationary excitation $f_{\text{am}}(t)$ is obtained on the basis of amplitude modulation, where first the stationary Gaussian signal $f(t)$ is generated and then it is multiplied by the modulating signal $m(t)$ with a specific non-stationarity rate. The stationary signal is considered as a carrier wave, whereas the modulating signal represents time-varying instantaneous power [11].

Stationary excitation is taken as a Gaussian random process realization with a prescribed flat-shape PSD in the frequency band from 100 to 150 Hz, as shown in Fig. 3a). The selected frequency band covers the natural frequency of the SDOF system, to which the excitation is applied. The corresponding stationary random-process realization is shown in Fig. 3b).

The modulating signals $m(t)$ of different non-stationarity rates are produced with the amplitude-modulation technique, where two groups of modulating signals are considered:

- modulating signals as random-process realizations with the prescribed flat-shape PSD [28],
- modulating signals obtained with a cubic spline interpolation of the points, produced by the use of a beta distribution [16].

In the first approach, modulating signals are obtained as absolute values of random process realizations, which ensure non-stationary excitation with an initial kurtosis $k_{\text{u}} > 3$. Excitation signal $f_{\text{am}}(t)$ is obtained as [40]:

$$f_{\text{am}}(t) = f(t)(|m(t)|^p + \Delta m), \quad (41)$$

where exponent p and tolerance Δm are introduced to provide a desired kurtosis of resulting signal. Values of both parameters can not be determined in advance, and iteration is needed to obtain excitation signal's kurtosis $k_{\text{u}} = 7$. To numerically research how the non-stationary excitation reacts with the structure, different excitation signals with modulation $m(t)$ frequency ranges were prepared using the Python open-source pyExSi package [46]: [0.001-0.01] Hz,

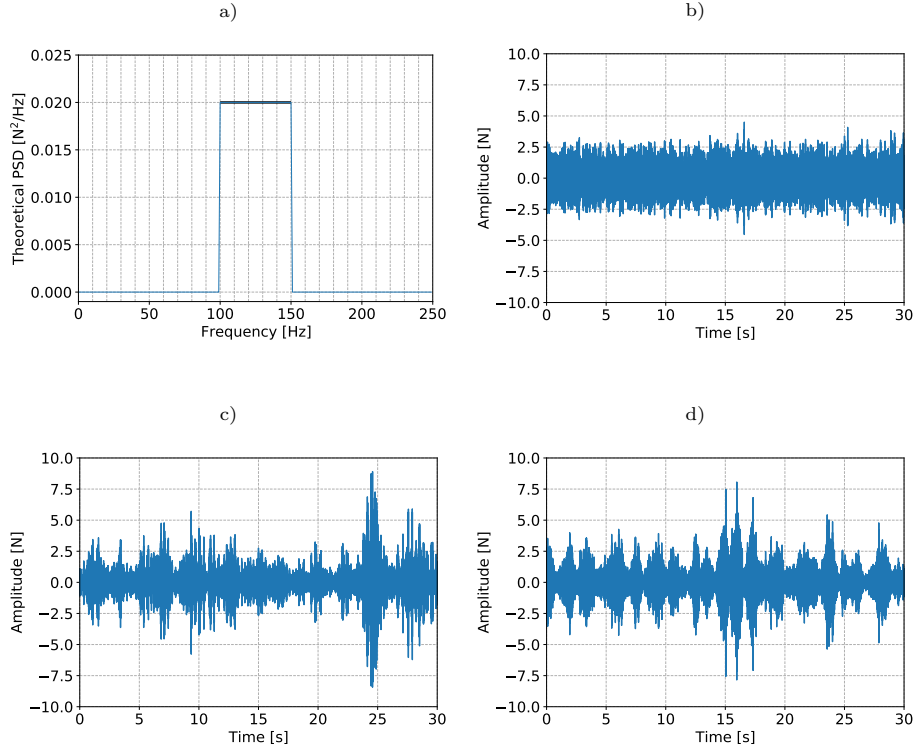


Figure 3: Excitation generation: a) PSD of stationary excitation with variance of 1 N^2 ; b) stationary excitation; c) non-stationary excitation FR-[1-2]; d) non-stationary excitation CS-4096

[0.01-0.1] Hz, [0.1-1] Hz, [1-2] Hz, [2-5] Hz, [5-10] Hz, [10-25] Hz, [25-50] Hz, [50-100] Hz and [100-200] Hz. Corresponding to the frequency range of modulation, the non-stationary excitation is labeled as FR- l . For example, the non-stationary excitation FR-[1-2], depicted in Fig. 3c), is significantly below the natural frequency of the later researched dynamic structure, while FR-[100-200] is in the same frequency range.

In the second approach, modulating signals $m(t)$ with the required non-stationarity rate are generated with a cubic spline interpolation of points, based

on a beta distribution, whose probability density function (PDF) is given as [34]:

$$p(x) = \frac{x^{\alpha-1}(1-x)^{\beta-1}\Gamma(\alpha+\beta)}{\Gamma(\alpha)\Gamma(\beta)}, \quad (42)$$

where $\Gamma(\cdot)$ represents gamma function. Parameters α and β are chosen in a way to obtain the desired kurtosis $k_u = 7$ of the resulting non-stationary excitation $f_{\text{am}}(t)$. In this approach, only first order properties of modulating signal are considered. The non-stationarity rate is affected by the number of points l used in the cubic spline interpolation, as the frequency of the modulation signal increases with the number of points l . The notation for the non-stationary loading is CS- l . The following non-stationary signals are generated: CS-16, CS-32, CS-128, CS-256, CS-512, CS-1024, CS-2048, CS-4096, CS-8192, CS-16384, CS-32768, CS-65536, CS-131072, CS-262144 and CS-524288. Signal synthesis is done with the pyExSi package [46]. Again, CS-16 is significantly below the natural frequency of the researched dynamic structure, while CS-524288 is in the same frequency range. Fig. 3d) shows the non-stationary excitation CS-4096.

For all the above-generated signals, a sampling frequency of 8096 Hz was used, with an excitation signal length of ≈ 35 min.

4.2. Numerical test case

For the numerical test case a SDOF system is used, as shown in Fig. 4a), with the natural frequency $f_r = 120$ Hz. For the sake of simplicity, the modal response $q_r(t)$ to excitation $f_{\text{am},r}(t)$ is considered as the r -th mode EVMS stress time history ${}_{r}{}_{s_c}(t)$ (30) (transformation from modal displacements to stresses can be carried out via a FEM analysis). For small values of the damping, the dynamic system approximates a narrowband filter, as can be seen from Fig. 4b).

To research the influence of the short-time Δt on the average short-time-based damage-intensity $\bar{d}_{\text{NB},\Delta t}$ estimation (38), the short-time Δt (using parameter n , Eq. (35)) *vs.* the modulation frequency of the non-stationary excitation and the damping ratio ξ is researched. The error in the damage estimation T_{err} is researched for both types of non-stationarity generation, see Figs. 5 and 6 for

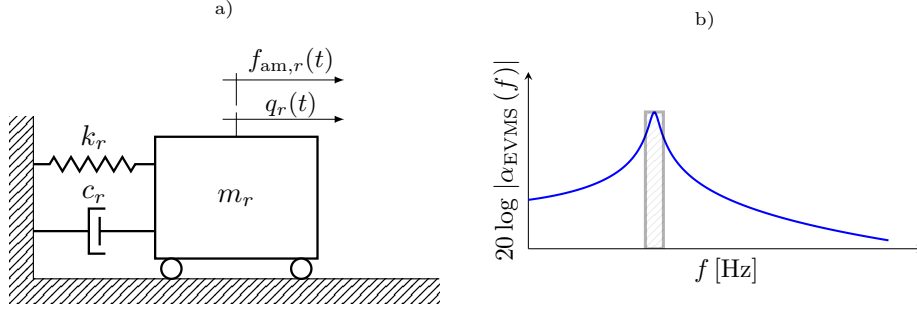


Figure 4: SDOF system: a) model; b) EVMS stress FRF

FR- l and CS- l , respectively. From the figures it is evident that there is a significant error in the identified damage at different short-time window parameter (n) used for different types of non-stationarity.

If closer attention is paid to the numerical results for the parameter $n \in [0.25, 3]$ and the damping ratio $\xi \in [0.001, 0.051]$, then the spread of the error is significantly reduced for both types of non-stationary excitation and for all the modulation parameters, see Fig. 7a) where the standard deviation of the fatigue-life error $\sigma_{T_{\text{err}}(\xi, n)}$ is shown. Fig. 7b) shows the standard deviation of the fatigue-life error averaged for all the damping ratios $\bar{\sigma}_{T_{\text{err}}(n)}$; from the figure it is clear that the minimum spread of the results is at $n = 0.75$. This corresponds to the short-time $\Delta t = T_w(\delta = 0.178)$, Eq. (34). While the proper δ was found (and later used) to be 0.178; based on the result shown in Fig. 7b), δ in the range from 0.1 to 0.5 (corresponding to $n \in [0.25, 1]$) would not have a significant influence on the standard deviation of the fatigue-life error.

Fig. 8 shows the averaged fatigue-life error for both groups of non-stationarity (averaged over all the modulation parameters); from the averaged results a close-to-linear dependency on the damping was observed. Due to the close-to-linear relation, a linear approximation of both types of non-stationarity was made $\bar{T}_{\text{err}, \text{lin}}(\xi)$ (approximation range $\xi \in [0.001, 0.051]$):

$$\bar{T}_{\text{err}, \text{lin}}(\xi) = -2.331 \xi - 0.431. \quad (43)$$

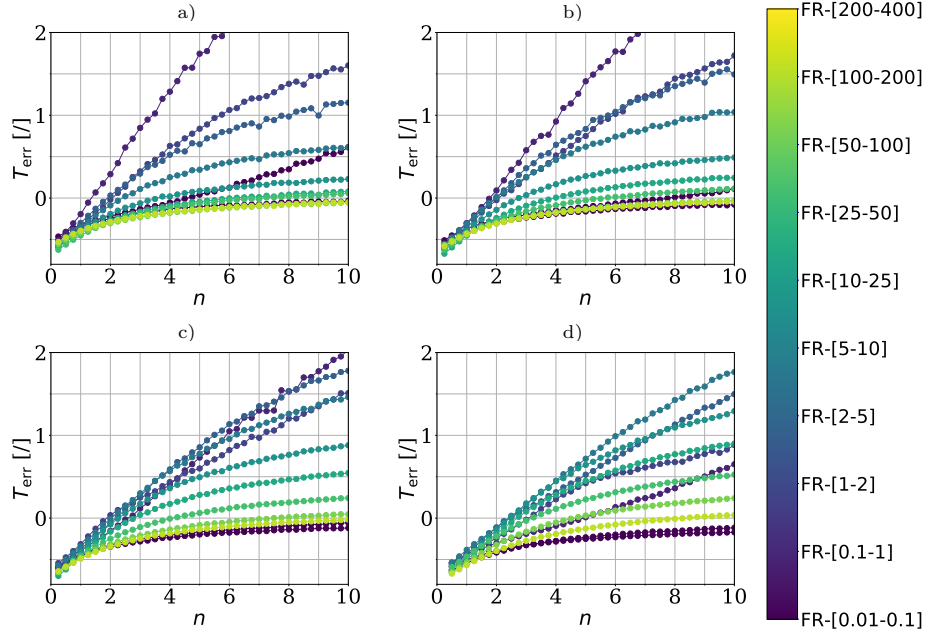


Figure 5: Fatigue-life error T_{err} for non-stationary excitation FR- l and various damping ratios ξ : a) $\xi=0.005$; b) $\xi=0.01$; c) $\xi=0.02$; d) $\xi=0.05$

For the purpose of identification of correct short-time-window width, multiple S-N curve slopes were used ($k \in [3 - 13]$). The Eq. (43) is identified for $k = 5.9$. A detailed analysis showed that the $\bar{T}_{\text{err},\text{lin}}$ is weakly exponentially dependent on k and can be in the range $k \in [3 - 13]$ defined as (see Appendix Appendix B for details):

$$\begin{aligned} \bar{T}_{\text{err},\text{lin}}(\xi, k) = & \left(2.297 e^{-\frac{k-3}{1.622}} + 2729.224 e^{\frac{k-3}{15658}} - 2732.392 \right) \cdot \xi \quad (44) \\ & + 0.756 e^{-\frac{k-3}{4.423}} - 0.826. \end{aligned}$$

A flowchart in Fig. 9 summarizes the short-time fatigue-life estimation. Considering Eq. (44), the average short-time fatigue-damage intensity $\bar{d}_{\text{NB},\Delta t}$ (38) can be corrected:

$$\bar{d}_{\text{NB},\Delta t}^{\text{cf}}(\xi, k) = \bar{d}_{\text{NB},\Delta t} \cdot (\bar{T}_{\text{err},\text{lin}}(\xi, k) + 1). \quad (45)$$

Based on Eqs. (39) and (45), the estimated fatigue life $\bar{T}_{\text{NB},\Delta t}^{\text{cf}}$ is compared

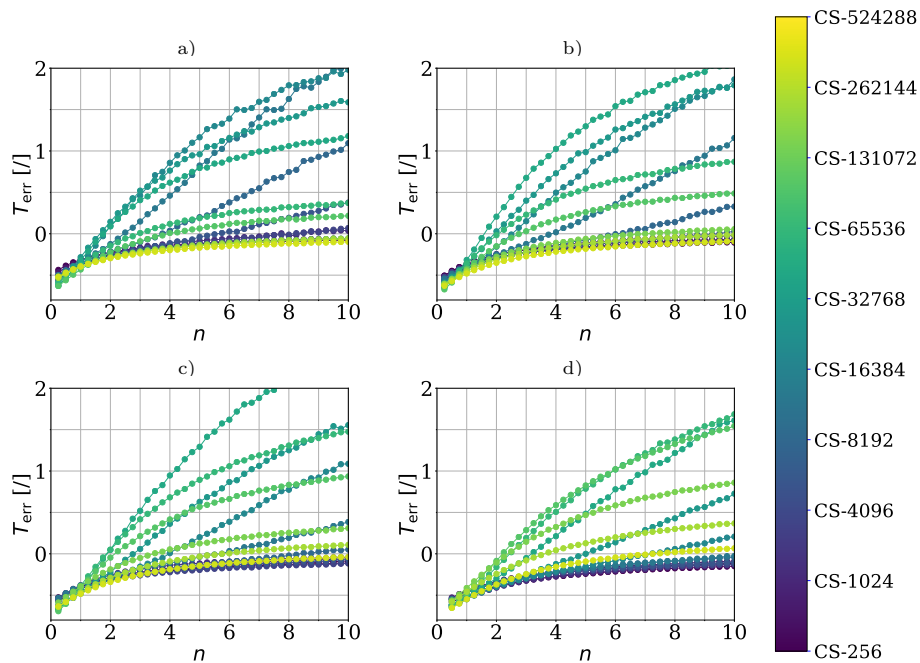


Figure 6: Fatigue-life error T_{err} for non-stationary excitation $CS-l$ and various damping ratios ξ : a) $\xi=0.005$; b) $\xi=0.01$; c) $\xi=0.02$; d) $\xi=0.05$

to the rainflow-counting-based fatigue life T_{RFC} for both types of non-stationary excitation (for $k = 5.9$), as depicted in Fig. 10. For reference, the fatigue life is evaluated with the narrowband spectral method [36], where stationarity of the excitation is assumed. In contrast to the narrowband spectral method, which over-estimates predicted fatigue life in case of non-stationary excitation, the proposed method allows for narrowband approximation under such non-stationary conditions.

5. Experiment

In this section a non-stationary excited structure is researched with the proposed short-time method (45); the numerical fatigue-life estimation is compared to the experimentally observed fatigue life. The experimental data are taken from the experiment presented by Capponi *et al.* [9]; where, in this re-

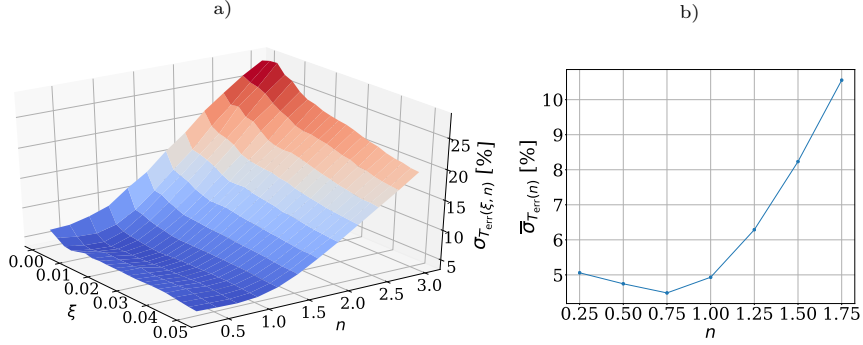


Figure 7: Standard deviation of fatigue-life error: a) $\sigma_{T_{\text{err}}(\xi, n)}$; b) $\bar{\sigma}_{T_{\text{err}}(n)}$, averaged over ξ

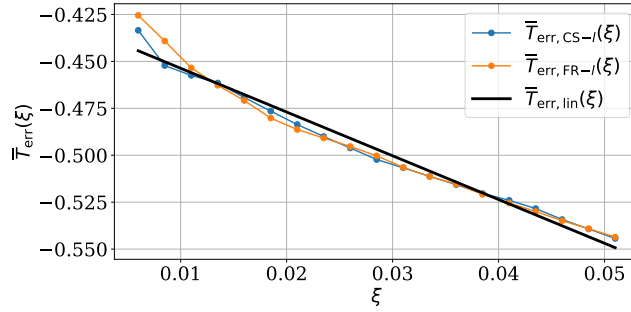


Figure 8: Average fatigue-life error $\bar{T}_{\text{err}}(\xi)$ vs damping ratio ξ

search, we have used additional acceleration response measurements which were previously not reported, neither used (see Fig. 11a)). Based on the additional measurement, the stress response time-history $r_{s_c}(t)$ is obtained as described in following paragraphs.

With accelerated fatigue testing on an electro-dynamic shaker, a large stress response can be achieved with little excitation power if the natural frequency of the test object lies in the excitation frequency range. For this purpose, a Y-shaped sample was taken as the test object [9], as it satisfies the prerequisites of well-separated natural frequencies in the excitation frequency range.

The Y-shaped sample (Fig. 11a)) consist of three beams at 120° around the main axis with a rectangular cross-section of $10 \times 10 \text{ mm}^2$. It was made

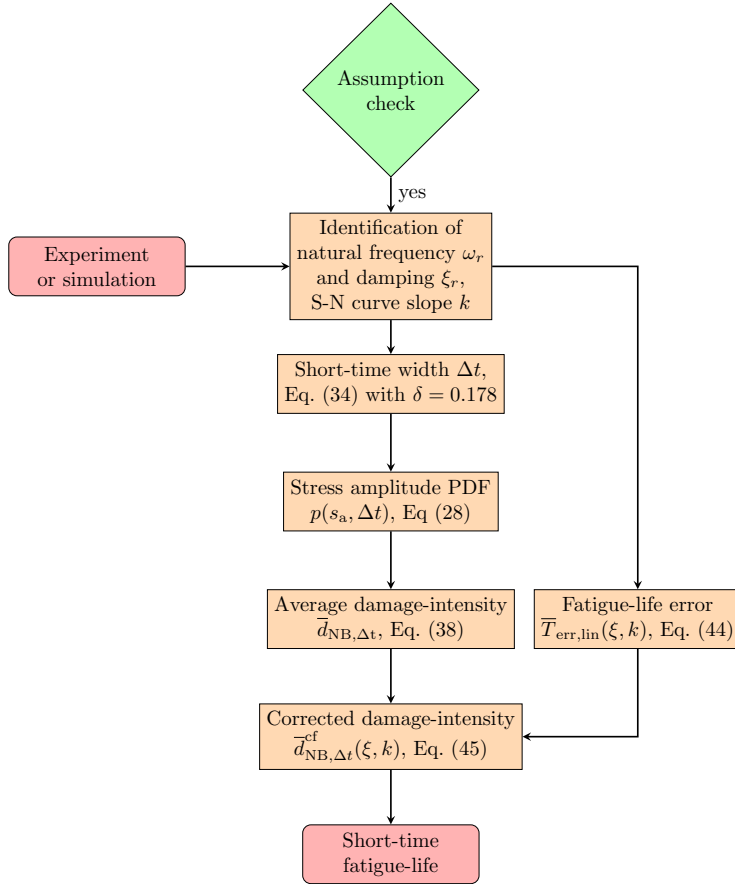


Figure 9: Flowchart of the short-time fatigue-life estimation.

from an aluminium alloy A-S8U3 casting with a density of 2710 kg/m^3 and a Young's modulus of $75\,000 \text{ MPa}$, with a surface finish produces by milling. As the surface finish is critical for a high-cycle fatigue life where crack initiation dominates the fatigue life [18], additional fine grinding was applied to the fatigue zone to reduce the surface roughness. With regard to an adequate excitation of the analyzed mode shape with translational movement in the shaker's axial direction, the 4-th mode shape, depicted in Fig. 11b), was considered as the most appropriate. To adjust the initial natural frequency of sample to $f_4 = 775 \text{ Hz}$, steel weights with a mass of 52.5 g were fixed to the ends of the two beams.

Fig. 11a) shows the Y-shaped sample, mounted on an LDS V555 electro-

dynamic shaker with a fixation adapter. Two accelerometers were used to measure the response to force excitation: PCB T333B30 for the base of the shaker (excitation) and Bruel&Kjær 4517-002 to measure the response of the tested sample. For the signal acquisition and generation, NI-9234 24-bit and NI-9263 16-bit ADC modules were used, respectively.

Non-stationary excitation signals were generated by multiplication of the stationary Gaussian random signal with modulating signals of different non-stationarity rates. Stationary Gaussian signal is defined with flat-shaped PSD in frequency band from 600-850 Hz, exciting 4-th natural frequency of Y-shaped sample. A modulating signal $m(t)$ with the desired non-stationarity rate is generated by squeezing the primary modulating signal. The latter is obtained with a cubic spline interpolation of the points, based on a beta distribution [16]. After squeezing the primary modulating signal l -times, and then by replicating and appending it to reach the total duration of the stationary signal, both signals can be multiplied. In this way a random non-stationary excitation with a specific non-stationarity rate is obtained, labeled SQ- l . The following non-stationary signals were generated: SQ-1, SQ-2, SQ-4, SQ-10, SQ-50, SQ-500 and SQ-10000. To perform comprehensive experimental testing, excitations at four different force PSD levels were carried out: 6.75, 9, 13.5 and 18 N²/Hz. Certain load cases (combination of force PSD level and signal type) were left untested or no failure after $2 \cdot 10^7$ load cycles was observed [9]. The sample failure was identified as a drop in the sample's 4-th natural frequency, for details see [9]. The experimentally observed fatigue life [s] is given in Tab. 1.

For each sample, full time histories of the excitation and response accelerometer were measured (sampling frequency: 25 600 Hz). The shortest time-history length of ≈ 6 min matches the excitation type SQ-4 at 18 N²/Hz, whereas in the case of the stationary excitation at a PSD level of 9 N²/Hz the time history exceeds 210 min. The total number of experiments was 42 and the total amount of measured data ≈ 100 GB. These measurements were used for the 4-th mode-shape hotspot stress time-history estimation. The stress time-history estimation was based on a numerical FEM modal model (as a linear system), which was

Force PSD level [N ² /Hz]		6.75		9		13.5		18	
Signal type	SQ-1	5112 7807	4865 7445	2364 3740	2994 3767	961	857 1666	-	
	SQ-2	2737 9522	4405 8389	2853 3538	2391 4327	871 1689	907 1616	-	
	SQ-4	4429 9681	5435 9625	3279 3992	2899 4288	737 1689	899 1674	643 726	341 947
	SQ-10	-		3177 5564	3824 5282	1175 2151	1333 2086	598 338	497 1179
	SQ-50	-		3722 11595	5894 12116	1120 3794	5234 3592	999 1666	1069 1706
	SQ-500	-		>12600		4069 4662	6411 4817	1624 2188	2793 2246
	SQ-10000	-		-		6299 4725	6309 5228	-	
	Stationary	-		>12600		4428 5416		3157 2573	

Table 1: Experimental (black) and numerically predicted (red) fatigue life [s] (for most load cases, two samples were tested)

used to identify the FRF to the EVMS stress time-history $r_{s_c}(t)$ (30); the input to the numerical model was the measured relative acceleration (response acceleration minus base acceleration). The 4-th natural frequency's corresponding stress mode shape hotspot is shown in Fig. 11b). Using Eq. (45) the fatigue life was estimated as the inverse of the damage intensity $\bar{d}_{\text{NB},\Delta t}^{\text{cf}}(\xi, k)$. In the damage estimation the experimentally identified damping ratio of the 4-th mode shape was used: $\xi_4 = 0.003$. The fatigue parameters were determined on the stationary excited samples using the least-square optimization; the narrowband spectral method was related to the experimentally identified fatigue life, result-

ing in:

$$k = 5.9, \quad C = 4.04 \cdot 10^{18} \text{ [MPa}^k\text{]}.$$

Based on the experimentally identified fatigue parameters, damping, natural frequencies and the time histories from both accelerometers, the fatigue life was obtained for each tested sample, see Tab. 1. Fig. 12 compares the narrow-band spectral method (which assumes stationarity) to the proposed short-time method; for non-stationary excitation a significant improvement in the fatigue life accuracy is observed. As the proposed method represents numerical simplification of more accurate time-domain modelling of fatigue process, Fig. 12c) depicts a comparison between rainflow-counting-based fatigue life T_{RFC} and experimental life.

For the estimation of the fatigue life $\bar{T}_{\text{NB},\Delta t}^{\text{cf}}$, shown in Fig. 12, the total length of the time-histories was used (until failure). In an application this does not make a lot of sense, as the fatigue damage should be estimated from the shortest-possible time histories. In non-stationary excitation, this is particularly hard to perform. Due to this, Fig. 13 shows the relative error of the estimated fatigue life as a function of the measured time, where the fatigue-life estimation with the total length of the time history was taken as a reference fatigue life. For clarity reasons, only selected load cases are shown: SQ-1, SQ-10, SQ-10000 and stationary loading (all excitation PSD level of $13.5 \text{ N}^2/\text{Hz}$). As expected, the stationary conditions converge faster than the non-stationary. For the non-stationary loads we observed that the rate of convergence is dependent on the modulating parameters of the loading, *i.e.*, the higher the modulating frequency in the non-stationarity, the faster the convergence of the fatigue life $\bar{T}_{\text{NB},\Delta t}^{\text{cf}}$.

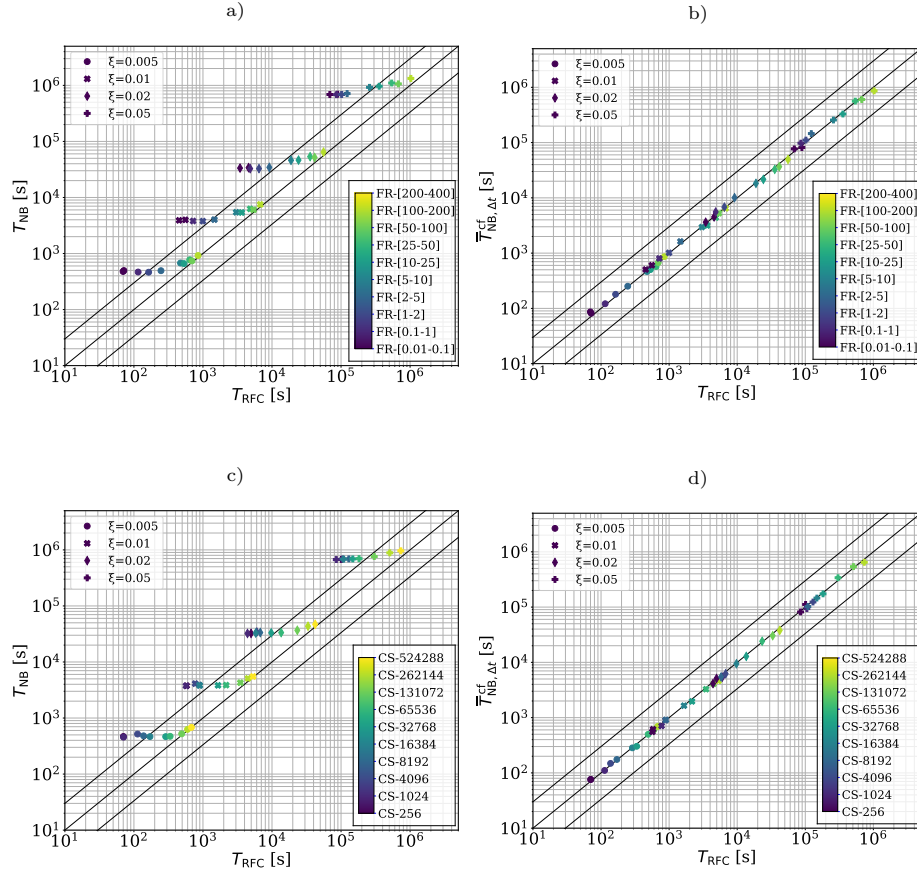


Figure 10: Numerically predicted fatigue life for non-stationary signals FR- l and CS- l : a) FR- l , narrowband spectral method; b) FR- l , the proposed method; c) CS- l , narrowband spectral method; d) CS- l , the proposed method

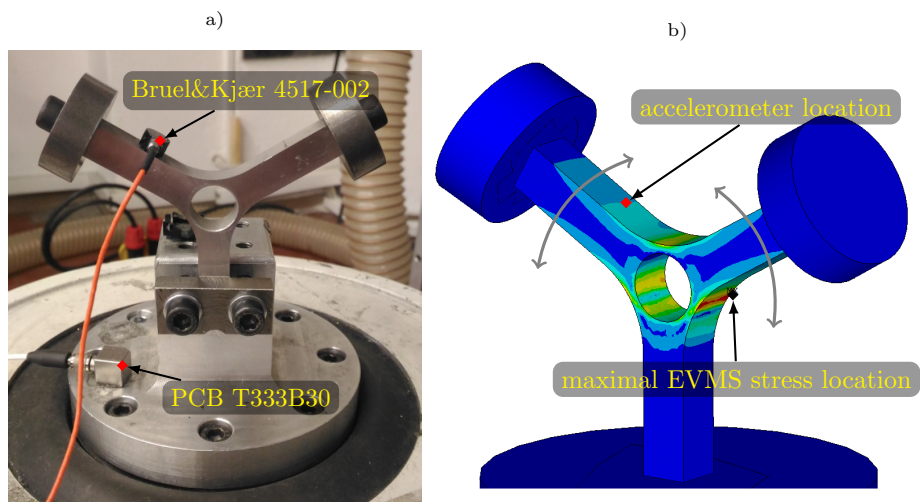


Figure 11: Y-shaped sample: a) with installed accelerometers [9]; b) FEM model of as mounted on the shaker's moving element, displaying EVMS stress location for the 4-th mode shape

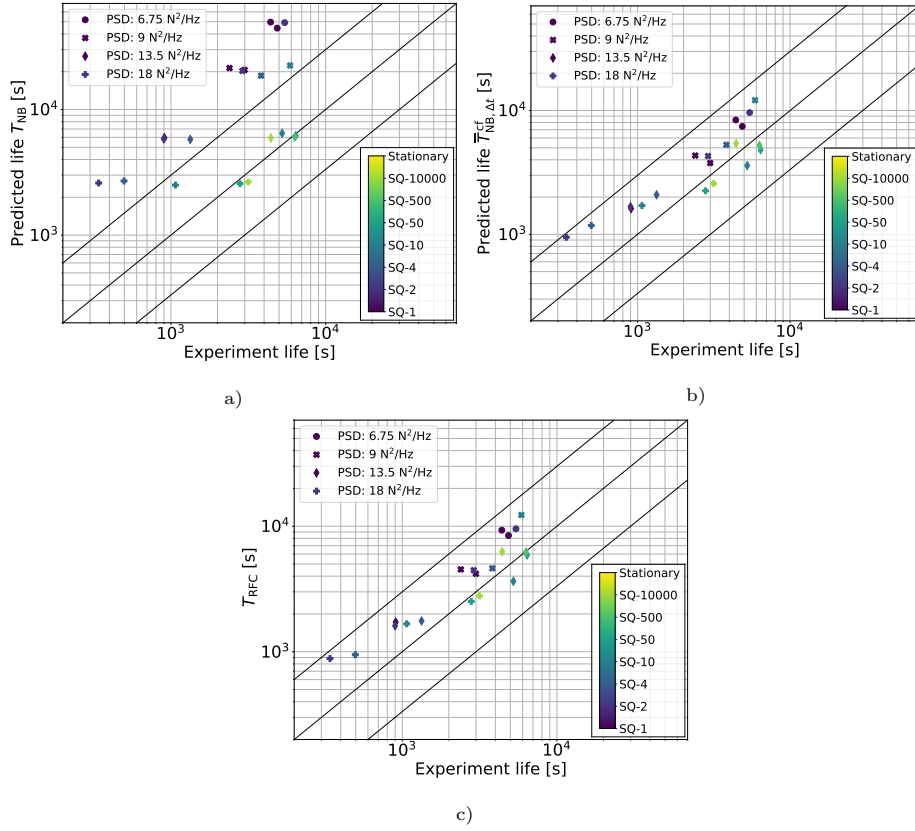


Figure 12: Experimental and predicted fatigue life: (a) using narrowband spectral method; (b) using proposed method; (c) rainflow-counting-based fatigue life T_{RFC}

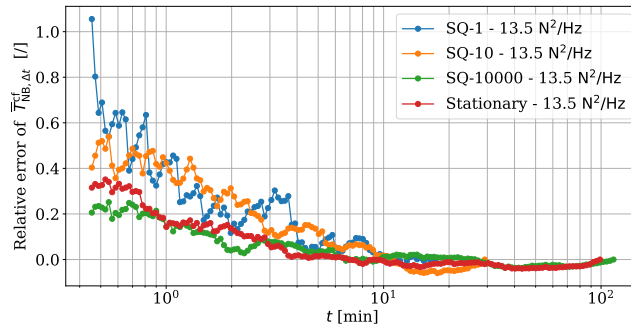


Figure 13: Relative error of the estimated fatigue life $\bar{T}_{NB,\Delta t}^{cf}$ as a function of the time-history length

6. Conclusions

This research focuses on the fatigue-life estimation of flexible structures exposed to non-stationary excitation. Non-stationarity propagates through the dynamic structure from the excitation to the response location. This propagation is defined by the dynamic properties of the structure. In this research, it was shown that the propagation depends on the type of non-stationarity, the modulation frequency in the non-stationarity, and the dynamic properties of the structure (*i.e.*, the damping and natural frequency).

A new, averaged short-time damage intensity for non-stationary excitation is introduced. The method is based on the narrowband spectral method and on the modal decomposition of the stress mode shapes. Due to the assumptions of the proposed method, it is only valid close to the localized mode shape hotspots; however, as flexible structures accumulate most fatigue damage in the natural frequencies, this is not limiting the applicability, provided the stress hotspots of different modes do not superimpose. One of the critical parameters is the time length in the short-time method, which is researched for two types of non-stationarity.

Numerical research is presented that reveals the importance of damping and natural frequency for a proper damage-intensity identification during non-stationary excitation. The experimental test case showed a significant improvement in the identification of the fatigue-life. If (for a non-stationary excited system) the stationarity assumption was used, the error was within the 800 percent range, while with the proposed averaged short-time damage intensity method, the error was within the 250 percent range. The results are promising in terms of providing a general framework for fatigue-life estimations of non-stationary excited dynamic structures.

Acknowledgements

The authors acknowledge the partial financial support from the Slovenian Research Agency (research core funding no. P2-0263 and project J2-1730).

References

- [1] D. S. 00-35. Environmental handbook for defense material. part 5:induced mechanical environments, 1999.
- [2] C. Amzallag, J. P. Gerey, J. L. Robert, and J. Bahuaud. Standardization of the rainflow counting method for fatigue analysis. *International Journal of Fatigue*, 6(4):287–293, 1994.
- [3] D. Benasciutti. An analytical approach to measure the accuracy of various definitions of the equivalent von mises stress in vibration multiaxial fatigue. In *Conference: International Conference on Engineering Vibration*, Ljubljana, Slovenia, 09 2015.
- [4] D. Benasciutti and R. Tovo. Cycle distribution and fatigue damage assessment in broad-band non-gaussian random processes. *Probabilistic Engineering Mechanics*, 20(2):115–127, 2005.
- [5] D. Benasciutti and R. Tovo. Frequency-based fatigue analysis of non-stationary switching random loads. *Fatigue & Fracture of Engineering Materials & Structures*, 30(11):1016–1029, 2007.
- [6] J. S. Bendat and A. G. Piersol. *Random Data: Analysis and Measurement Procedures*. Wiley India, 2013.
- [7] C. Braccesi, F. Cianetti, G. Lori, and D. Pioli. The frequency domain approach in virtual fatigue estimation of non-linear systems: The problem of non-gaussian states of stress. *International Journal of Fatigue*, 31:766–775, 2009.
- [8] L. Capponi, J. Slavič, G. Rossi, and M. Boltežar. Thermoelasticity-based modal damage identification. *International Journal of Fatigue*, 137:105661, 2020.
- [9] L. Capponi, M. Česnik, J. Slavič, F. Cianetti, and M. Boltežar. Non-stationarity index in vibration fatigue: Theoretical and experimental research. *International Journal of Fatigue*, 104:221–230, 2017.

- [10] A. Carpinteri, A. Spagnoli, and S. Vantadori. A review of multiaxial fatigue criteria for random variable amplitude loads. *Fatigue & Fracture of Engineering Materials & Structures*, 40(7):1007–1036, 2017.
- [11] L. F. Chaparro and A. Akan. *Signals and Systems Using MATLAB*. Academic Press, 2019.
- [12] F. Cianetti. How to experimentally monitor the fatigue behaviour of vibrating mechanical systems. *Journal of Mechanical Engineering*, 66:557–566, 2020.
- [13] F. Cianetti, M. Palmieri, C. Braccesi, and G. Morettini. Correction formula approach to evaluate fatigue damage induced by non-gaussian stress state. *Journal of Sound and Vibration*, 8:390–398, 2018.
- [14] T. Dirlik. *Application of Computers in Fatigue Analysis*. PhD thesis, University of Warwick, 1985.
- [15] J. Enzweiler Marques, D. Benasciutti, and R. Tovo. Variability of the fatigue damage due to the randomness of a stationary vibration load. *International Journal of Fatigue*, 141:105891, 2020.
- [16] F. Kihm, S. A. Rizzi, N. S. Ferguson, and A. Halfpenny. Understanding how kurtosis is transferred from input acceleration to stress response and its influence on fatigue life. In *Proceedings of the XI International Conference on Recent Advances in Structural Dynamics*, Pisa, Italy, 07 2013.
- [17] T. Kranjc, J. Slavič, and M. Boltežar. A comparison of the strain and the classic experimental modal analysis. *Journal of Vibration and Control*, 22(2):371–381, 2016.
- [18] Y.-L. Lee, J. Pan, R. Hathaway, and M. Barkey. *Fatigue Testing and Analysis: Theory and Practice*. Butterworth-Heinemann, 2005.
- [19] F. Li, H. Wu, and P. Wu. Vibration fatigue dynamic stress simulation under non-stationary state. *Mechanical Systems and Signal Processing*, 146:107006, 2021.

- [20] N. M. M. Maia and J. M. M. Silva. *Theoretical and Experimental Modal Analysis*. Research Studies Press, 1997.
- [21] S. Mallat. *A Wavelet Tour of Signal Processing, Third Edition: The Sparse Way*. Academic Press, 2008.
- [22] M. Matsuishi and T. Endo. Fatigue of metals subjected to varying stress. *Japan Society of Mechanical Engineers*, 68:37–40, 1968.
- [23] M. Miner. Cumulative damage in fatigue. *Journal of Applied Mechanics*, 12:A159–A164, 1945.
- [24] G. Morettini, C. Braccesi, F. Cianetti, and S. M. J. Razavi. Design and implementation of new experimental multiaxial random fatigue tests on astm-a105 circular specimens. *International Journal of Fatigue*, 142:105983, 2021.
- [25] M. Mršnik, J. Slavič, and M. Boltežar. Frequency-domain methods for a vibration-fatigue-life estimation - application to real data. *International Journal of Fatigue*, 47:8–17, 2013.
- [26] M. Mršnik, J. Slavič, and M. Boltežar. Multiaxial vibration fatigue – a theoretical and experimental comparison. *Mechanical Systems and Signal Processing*, 76–77:409–423, 2016.
- [27] M. Mršnik, J. Slavič, and M. Boltežar. Vibration fatigue using modal decomposition. *International Journal of Fatigue*, 98:548–556, 2018.
- [28] D. E. Newland. *An Introduction to Random Vibrations, Spectral & Wavelet Analysis*. Dover Publications, 2005.
- [29] A. Niesłony, M. Böhm, and R. Owsński. Formulation of multiaxial fatigue failure criteria for spectral method. *International Journal of Fatigue*, 135:105519, 2020.
- [30] A. Palmgren. Die lebensdauer von kugellagern. *VDI-Zeitschrift*, 68:339–341, 1924.

- [31] M. Palmieri, M. Česnik, J. Slavič, F. Cianetti, and M. Boltežar. Non-gaussianity and non-stationarity in vibration fatigue. *International Journal of Fatigue*, 97:9–19, 2017.
- [32] X. Pitoiset and A. Preumont. Spectral methods for multiaxial random fatigue analysis of metallic structures. *International Journal of Fatigue*, 22(7):541–550, 2000.
- [33] A. Preumont and V. Piefort. Predicting random high-cycle fatigue life with finite elements. *Journal of vibration and acoustics*, 116(2):245–248, 1994.
- [34] V. K. Rohatgi and A. K. M. E. Saleh. *An Introduction to Probability and Statistics, 3rd Edition*. John Wiley & Sons, Inc., 2015.
- [35] V. Rouillard and M. A. Sek. Simulation of non-stationary vehicle vibrations. *Proceedings of the Institution of Mechanical Engineers, Part D: Journal of Automobile Engineering*, 215:1069–1075, 2001.
- [36] I. Rychlik. On the ‘narrow-band’ approximation for expected fatigue damage. *Probabilistic Engineering Mechanics*, 8(1):1–4, 1993.
- [37] K. Shin and J. K. Hammond. *Fundamentals of Signal Processing for Sound and Vibration Engineers*. John Wiley & Sons Ltd, 2008.
- [38] J. Slavič, M. Mršnik, M. Česnik, J. Javh, and M. Boltežar. *Vibration Fatigue by Spectral Methods*. Elsevier, 2020.
- [39] R. Tovo. Cycle distribution and fatigue damage under broad-band random loading. *International Journal of Fatigue*, 24(11):1137–1147, 2002.
- [40] A. Trapp, M. J. Makua, and P. Wolfsteiner. Fatigue assessment of amplitude-modulated non-stationary random vibration loading. *Procedia Structural Integrity*, 17:379—386, 2019.
- [41] A. Trapp and P. Wolfsteiner. Characterizing non-gaussian vibration loading using the trispectrum. *Journal of Physics: Conference Series*, 1264:012040, 2019.

- [42] A. Trapp and P. Wolfsteiner. Assessment of non-stationary random vibration loading. In *VAL4 - Fourth International Conference on Material and Component Performance under Variable Amplitude Loading*, pages 143–153, Darmstadt, Germany, 2020.
- [43] P. Wolfsteiner. Fatigue assessment of non-stationary random vibrations by using decomposition in gaussian portions. *International Journal of Mechanical Sciences*, 127, 2016.
- [44] P. Wolfsteiner and A. Trapp. Fatigue life due to non-gaussian excitation – an analysis of the fatigue damage spectrum using higher order spectra. *International Journal of Fatigue*, 127:203–216, 2019.
- [45] Y. Zhou and J. Tao. Theoretical and numerical investigation of stress mode shapes in multi-axial random fatigue. *Mechanical Systems and Signal Processing*, 127:499–512, 2019.
- [46] A. Zorman, D. Gorjup, and J. Slavič. `ladisk/pyexsi`: Release of the version v0.4, jan 2021.

Appendix A. Narrowband approximation

Closed-loop expression for narrowband approximation is given as [36]:

$$d_{\text{NB}} = \nu_0^+ C^{-1} \left(\sqrt{2} \sigma^2 \right)^k \Gamma \left(1 + \frac{k}{2} \right), \quad (\text{A.1})$$

where ν_0^+ is expected frequency of positive zero-crossings and $\Gamma(\cdot)$ represents gamma function. In numerical research, average damage intensity $\bar{d}_{\text{NB}, \Delta t}$ is implemented according to Eq. (38), but could be also done by time-averaging (denoted by $\langle \cdot \rangle$) of Eq. (A.1).

Appendix B. Fatigue-life error

The function for $\bar{T}_{\text{err,lin}}(\xi, k)$ (44) can be written as:

$$\bar{T}_{\text{err,lin}}(\xi, k) = A(k) \cdot \xi + B(k). \quad (\text{B.1})$$

A detailed analysis of the terms $A(k)$ and $B(k)$ has shown weak exponential dependence, see Figs. Appendix B.1a) and Appendix B.1b), respectively. Due to the exponential dependence, the exponential fit of data resulted in the Eq. (44).

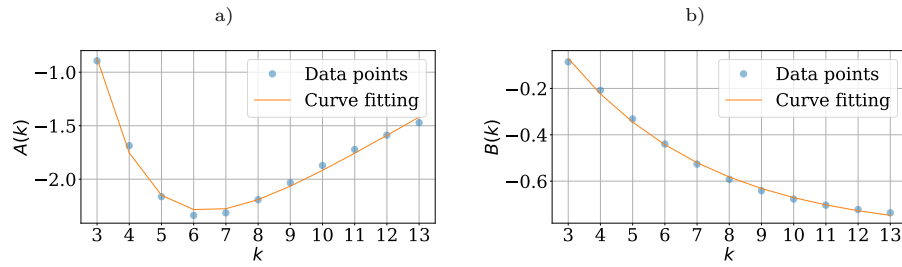


Figure Appendix B.1: Exponential fit of data: a) $A(k)$; b) $B(k)$